AD-A114 208 MICHIGAN TECHNOLOGICAL UNIV HOUGHTON DEPT OF METALLU--ETC F/G 11/6
ANNUAL TECHNICAL REPORT TO THE OFFICE OF NAVAL RESEARCH.(U)
NOV 81 D A KOSS N00014-76-C-0037

UNCLASSIFIED NL

10

ANNUAL TECHNICAL REPORT

TO

THE OFFICE OF NAVAL RESEARCH

CONTRACT No. N00014-76-C-0037, NR 031-756

BY

D. A. KOSS

DEPARTMENT OF METALLURGICAL ENGINEERING
MICHIGAN TECHNOLOGICAL UNIVERSITY
HOUGHTON, MICHIGAN U.S.A.

SECURITY CLASSIFICATION OF THIS PAGE (When Data Entered)

REPORT DOCUMENTATION PAGE		READ INSTRUCTIONS BEFORE COMPLETING FORM
1. REPORT NUMBER	2. GOVT ACCESSION NO. AD-A114 208	3. RECIPIENT'S CATALOG NUMBER
4. TITLE (and Subtitle) Annual Technical Report		5. TYPE OF REPORT & PERIOD COVERED Annual 10/1/80 - 9/30/81
		6. PERFORMING ORG. REPORT NUMBER
7. AUTHOR(s) D. A. Koss		8. CONTRACT OR GRANT NUMBER(s) N00014-76-C-0037 NR031-756
9. PERFORMING ORGANIZATION NAME AND ADDRESS Department of Metallurgical Engineering Michigan Technological University Houghton, MI 49931		10. PROGRAM ELEMENT, PROJECT, TASK AREA & WORK UNIT NUMBERS
11. CONTROLLING OFFICE NAME AND ADDRESS Office of Naval Research Department of the Navy Arlington, VA 22217		12. REPORT DATE Nov. 1981
		13. NUMBER OF PAGES 23
14. MONITORING AGENCY NAME & ADDRESS(if different from Controlling Office)		15. SECURITY CLASS. (of this report) Unclassified
		15a. DECLASSIFICATION/DOWNGRADING SCHEDULE

16. DISTRIBUTION STATEMENT (of this Report)

Distribution of this document is unlimited.

17. DISTRIBUTION STATEMENT (of the abstract entered in Block 20, if different from Report)

18. SUPPLEMENTARY NOTES

19. KEY WORDS (Continue on reverse side if necessary and identify by block number)

Ti alloys, texture, plastic anisotropy, deformation, hydrogen embrittlement, fracture, multiaxial stress states

20. ABSTRACT (Continue on reverse side if necessary and identify by block number)

Progress is reviewed in a research program directed at the influence of microstructure (especially texture) and hydrogen on the deformation and fracture behavior of wrought α, α-β and β Ti alloys in the form of sheet and tubing under both uniaxial and multiaxial states of stress. Specifically, the research involves:

1) a study of the deformation and fracture of strongly textured Ti alloy sheet in: (a) uniaxial tension and (b) multiaxial tension,

DD FORM 1 JAN 73 1473 EDITION OF 1 NOV 65 IS OBSOLETE
S/N 0102-014-6601

SECURITY CLASSIFICATION OF THIS PAGE (When Data Entered)

20. Abstract (cont'd)

2) an analysis of localized necking in sheet containing an imperfection inclined to the major principal stress axis,

3) the development of a fracture limit diagram for determining hydrogen embrittlement of sheet under multiaxial loading conditions,

4) a study of hydrogen embrittlement of Ti sheet under multiaxial deformation,

5) an examination of the effect of hydrogen on the multiaxial stress-strain behavior of Ti tubing, and

6) an initial effort to determine the sensitivity of a β-phase Ti alloy, Ti-30V, to hydrogen embrittlement under multiaxial deformation.

DEFORMATION AND FRACTURE OF TITANIUM

Introduction

In service operation of Ti alloy components depends critically on their deformation and fracture properties under the operating state of stress and environment. Thus, understanding the deformation fracture behavior (including environmental interactions) under complex states of stress becomes essential as a basis not only for improving these properties by heat treatment or processing variables but also for the fail safe utilization of Ti alloys. Our present research has been directed at the influence of microstructure (especially texture) and hydrogen on the deformation and fracture behavior of wrought α, α-β and β Ti alloys in the form of sheet and tubing under both uniaxial and multiaxial states of stress. As will be briefly reviewed, substantial progress has been accomplished in these studies by this program in the period Oct. 1, 1980 to Sept. 30, 1981. These efforts involve:

1) a study of the deformation and fracture of strongly textured Ti alloy sheet in: (a) uniaxial tension and (b) multiaxial tension,
2) an analysis of localized necking in sheet containing an imperfection inclined to major principal stress axis,
3) the development of a fracture limit diagram for determining hydrogen embrittlement of sheet under multiaxial loading conditions,
4) a study of hydrogen embrittlement of Ti sheet under multiaxial deformation,
5) an examination of the effect of hydrogen on the multiaxial stress-strain behavior of Ti tubing, and
6) an initial effort to determine the sensitivity of a β-phase Ti alloy, Ti-30V, to hydrogen embrittlement under multiaxial deformation.

A significant aspect of this program is the educational experience which it provides to the graduate students involved. In the past fiscal year the program has supported: Dr. Kwai Chan (now at Stanford University) as well as Roy Bourcier, Charles Lentz, and Barbara Lograsso, all currently graduate students in the Department of Metallurgical Engineering. Degrees awarded within the last year to students supported by this program are: Kwai Chan, Ph.D., Roy Bourcier, M.S., and Lee Petzold, M.S.

1) Deformation and Fracture of Strongly Textured Ti Alloy Sheet: (a) Uniaxial Tension and (b) Multiaxial Tension
(with K. S. Chan, currently at Dept. of Mat'l Sci. and Eng., Stanford Univ., Stanford, CA)

Titanium alloys in sheet form usually possess crystallographic texture which, in some instances, can be quite strong. Crystallographic textures form in Ti alloy sheet because of the limited slip systems available in the hcp -phase as well as the large amount of deformation that is usually accompanied with processing sheet metal by rolling. In sheet deformation studies, crystallographic texture is usually related to a continuum plasticity parameter, R, which is a measure of material's plastic anisotropy and is defined as the ratio of width strain to thickness strain in a uniaxial tensile test. Despite extensive studies of biaxial yield stress increases in textured Ti sheet and of the control of the R-value by texture, there has been no detailed study of the influence of crystallographic texture on the large strain deformation and plastic instability process which results in localized necking* and subsequently, fracture in Ti alloys. There have been formability studies (1,2) which have examined certain effects of strain hardening, strain rate sensitivity, strain rate and temperature on the limit strains at the onset of localized necking (forming limits) of Ti and Ti-6Al-4V sheet. However, the sheet materials used in these investigations do not possess strong texture; the R-values are relatively constant (R 0.6 to 1.0).

The phenomenon of localized necking in sheet metal has been studied in considerable detail in steel, brass, aluminum alloys (see, for example, ref. 3). It is well established in these materials that strain hardening and strain rate sensitivity are both important in enhancing the resistance to localized

*Localized necking refers to a necking process in sheet material wherein material within a narrow trough or neck continues deforming while adjacent material ceases to deform. It is localized necking (not diffuse necking which occurs at maximum load) which usually limits the ductility of sheet.

necking and thus the formability. The influence of crystallographic texture and R-value on the stretch formability is, however, less conclusive. The difficulty lies in manipulating sheet metal processing to vary the R-value over a large range of values without changing other properties such as strain hardening exponent, n, and the strain-rate sensitivity emponent, m. In addition, owing to the nature of slip in fcc and bcc metals, the range of R-value studied is not large; usually $0.5 \leq R \leq 2$. It is therefore difficult to separate the effect of crystallographic texture and R-value from that of n and m.

This investigation has examined the influence of crystallographic texture on the process of strain localization and the subsequent localized necking and fracture behavior of strongly textured Ti-6Al-4V (Ti-6-4) and Ti-5Al-2.5 Sn (Ti-5-2.5). The tests are based on material with two distinctly different textures: (1) basal texture (basal poles are aligned parallel to the sheet normal and (2) basal transverse (basal poles are aligned in the transverse direction of the sheet). Photo-grided specimens have been used throughout so that detailed strain measurements can be made in order to determine the effect of the R-value on the development of localized necking as well as on the magnitudes of the forming limit and fracture strains. Manipulating the crystallographic texture of the Ti-alloy sheet to yield a wide range of R-values but with relatively constant n and m values, the influence of the R-value on the strain localization process has been separated from that due to strain hardening and strain rate sensitivity (i.e., n and m).

A. Behavior in Uniaxial Tension

The effects of crystallographic texture on the tensile yield stress, the work hardening exponent ($n = \frac{d\ln\sigma}{d\ln\varepsilon}$), strain-rate sensitivity exponent ($m = \frac{d\ln\sigma}{d\ln\dot{\varepsilon}}$), and plastic anisotropy parameter (R) for Ti-6-4 and Ti-5-2.5 are shown in Fig. 1. These may depend on the orientation of the stress axis in the

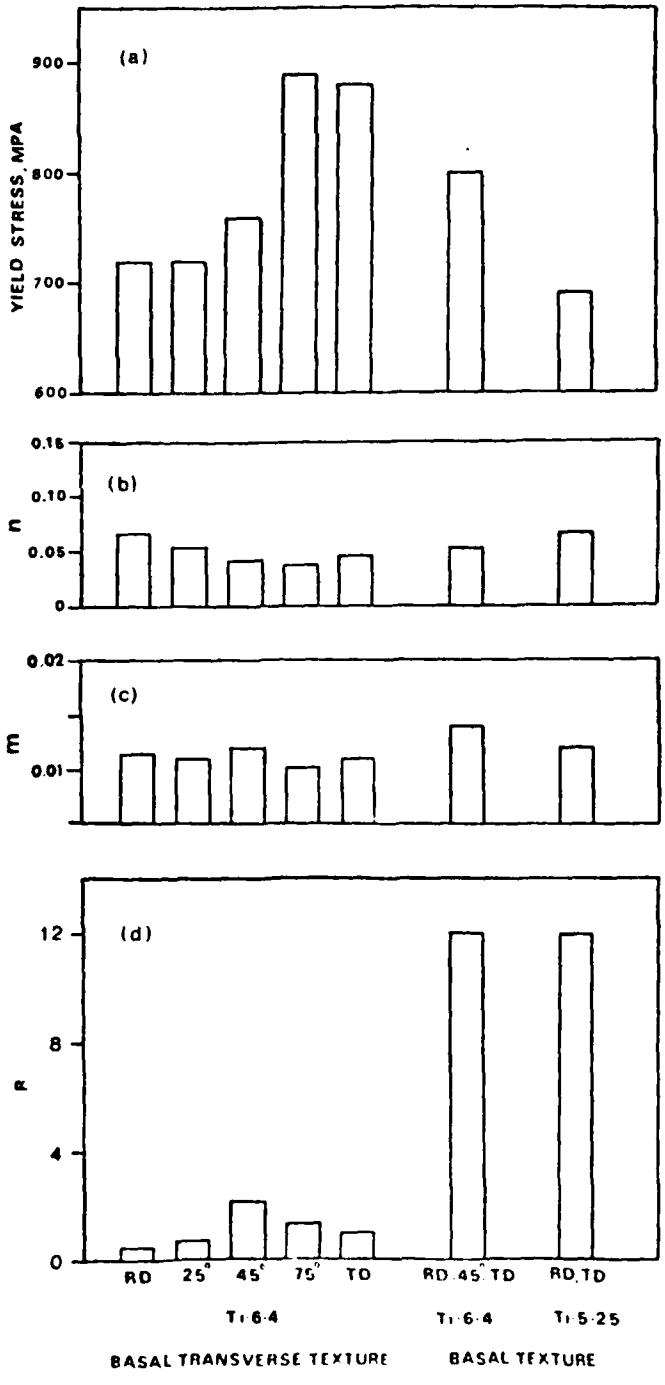

Fig. 1. The effects of crystallographic texture on the behavior of Ti-6Al-4V and Ti-5Al-2.5 Sn sheet for: (a) the yield stress, (b) the work hardening exponent n, (c) the strain rate hardening exponent m, and the plastic anisotropy parameter R.

basal-transverse textured sheet. An especially noteworthy result is that the influence of crystallographic texture on the work hardening exponent (n) and the strain rate sensitivity (m) is small when compared to the large changes in the plastic anisotropy parameter, R. The n and m values of the textured Ti-6-4 and Ti-5-2.5 sheet are relatively constant ($n \simeq 0.5$, $m \simeq 0.014$), while the R-value changes from 0.5 to 12. It should also be noted that the uniaxial yield stress of the basal-transverse Ti-6-4 depends strongly on specimen orientation with the TD (or near-TD) specimens having 25% higher yield stress than those tested parallel to or near the TD.

The dependence of plastic instability and fracture on the crystallographic texture is reflected in the influence of R-value on post-uniform elongation ε_{pu}, the limit strain ε_{ℓ}^{*} at the onset of localized necking, the fracture strain ε_{1f}, and the normalized fracture load P_f/P_{max}. As shown in Fig. 2, a high R-value is beneficial in enhancing post-uniform elongation, the limit strain, and in retaining the load-carrying capacity by increasing the fracture strain. In contrast, the R-value has little effect on the uniform strain ε_u for the onset of diffuse necking; ε_u depends mainly on the work hardening exponent, n, consistent with the Considere criterion for dissuse necking.

Analysis of photogridded test specimens reveals that the strain distribution within the tensile neck is strongly affected by the crystallographic texture through its pronounced influence on the R-value. The strain state within the tensile neck has been found to deviate from that of uniaxial tension and shift towards that of plane strain. This change of strain state results in additional hardening at the center of the diffuse neck. The amount of additional hardening increases with R, and, as a result, tensile neck becomes broader and more diffuse and the limit strain (at the onset of localized necking) is increased as the R-value is increased. Consequently, the post-uniform elongation, the fracture strain, and the ability to retain the load

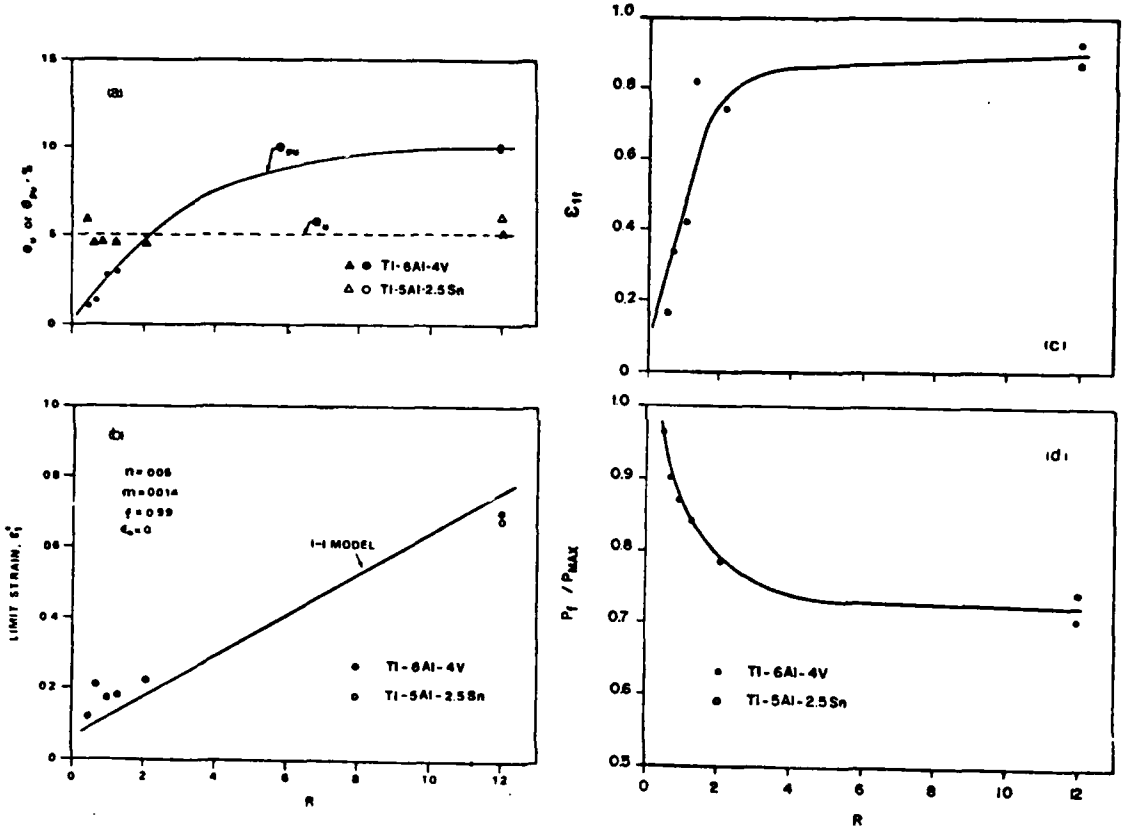

Fig. 2. The influence of the plastic anisotropy parameter R (= $\varepsilon_{width}/\varepsilon_{thickness}$) on: (a) the uniform ε_u or post-uniform ε_{pu} strain, (b) the limiting strain at the onset of localized necking ε_ℓ^*, (c) the major principal strain at fracture ε_{1f}, and (d) the load carrying capacity (= load at fracture/maximum load.)

carrying capacity after maximum load are all enhanced with increasing R-value. In addition, the theoretical calculations of forming limit strain using an inclined perfection model (4) are in good agreement with the experimental results and predict the enhancement in the limit strain with increasing R-value.

B. Behavior in Multiaxial Tension

In order to examine the influence of texture and plastic anisotropy on the localized necking of Ti-6Al-4V sheet, punch-stretch testing has been used. This technique involves the stretching of clamped, gridded sheet over a usually hemispherical punch (5-7). At failure (usually by a localized necking process), measurement of the grid elements near to the fractured surface allow one to determine the principal strain components in the plane of the sheet at the onset of localized necking $\varepsilon_{1\ell}$ and $\varepsilon_{2\ell}$. Given different degrees of lubrication between the punch and the die as well as differing specimen widths, the punch stretching technique may be used to obtain values of $\varepsilon_{1\ell}$ and $\varepsilon_{2\ell}$ for any multiaxial deformation path associated with thinning of the sheet. Such data is usually plotted in the form of a forming limit curve (FLC) which maps in strain space (ε_1 and ε_2) the strains at which localized necking occurs.

Using punch-stretch testing, the influence of crystallographic texture and R-value on the localized necking and fracture behavior of strongly textured Ti-6Al-4V and Ti-5Al-2.5 Sn sheet. Material with a strong basal as well as a strong basal-transverse texture was tested. Plotted in the form of forming limit curves, see Fig. 3, the punch-stretch results show the localized necking behavior in strongly textured Ti alloy sheet is very sensitive to loading path. In basal textured sheet with a high R-value (12) and therefore difficult through-thickness slip, Fig. 3 shows that the major principal strain of the onset of localized necking is reduced from 0.68 at uniaxial tension to 0.04 at balanced biaxial tension. In addition, a comparison of the FLC in this material

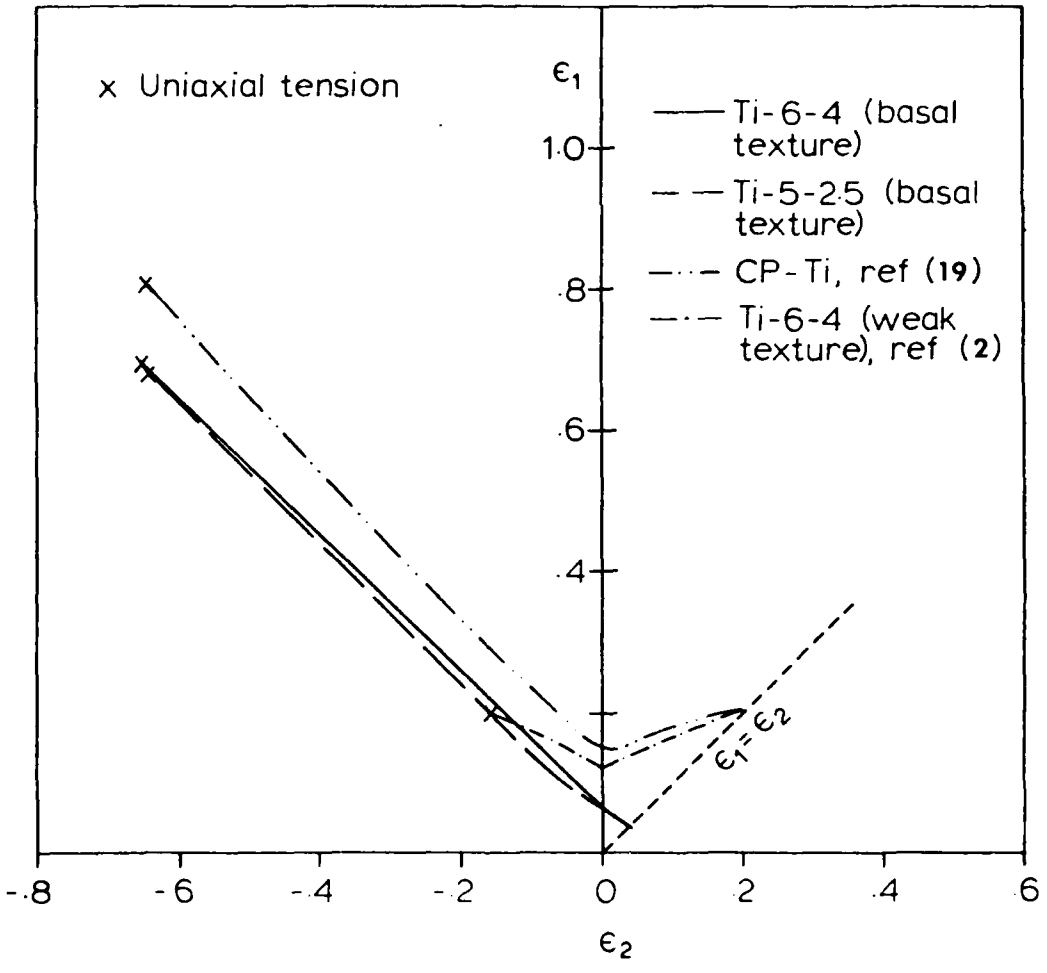

Fig. 3. The forming limit diagrams for: Ti-6Al-4V and Ti-5Al-2.5 Sn with a strong basal texture (>4 x random), commercially pure Ti with a strong (4.5 x random) CP texture and Ti-6Al-4V with a weak texture.

with that for a relatively isotropic Ti-6Al-4V sheet with similar n and m values (see Fig. 3) shows that a high R-value improves resistance to localized necking only in the negative minor strain regions ($\varepsilon_2<0$) of the FLC. These data also indicate that a low R-value offers better limit strains in the positive minor strain regime ($\varepsilon_2>0$). The R-value appears to have no effect on localized necking at plant strain ($\varepsilon_2 = 0$).

The forming limit curves of the Ti-6Al-4V sheet with basal transverse texture are orientation dependent. In the $\varepsilon_2<0$ regime, the limit strains in the TD exceed those in the RD, probably due to a higher R-value (R = 1.0 in the TD vs 0.5 in the RD). In the $\varepsilon_2>0$ region, localized necking occurs exclusively along a line normal to the TD and comparison to the RD behavior is not possible. Since the R-value is higher in the TD, these observations are also consistent with the trend that increasing R improves the resistance to localized necking in the $\varepsilon_2<0$ of the FLC but has the reverse effect in the $\varepsilon_2>0$ region. A complicating factor is the possibility that fracture might affect the FLC for $\varepsilon_2>0$ in the sheet with planar anisotropy.

2) Localized Necking: An Inclined Imperfection Model
(with K. S. Chan, currently at Dept. of Mat'l. Sci. and Eng., Stanford Univ., Stanford, CA and A. K. Ghosh, Science Center, Rockwell International, Thousand Oaks, CA)

Sheet materials deforming under multiaxial states of stress, as in sheet metal forming operations, usually fail by localized necking. The current interest in understanding sheet metal formability has led to several theoretical analyses of localized necking based on different criteria. These localized necking criteria include: a localized shear zone along a direction of zero-extension (8), material imperfections (9), or the presence of a vertex on the yield surface (10), and void growth (11).

Strain localization developed by local weakness of material was first proposed by Marciniak and Kyczynski (M-K)(9) and extended by Sowerby and

Duncan (12). In the M-K analysis, a material imperfection exists normal to the principal strain (ε_1). Imposing the same ε_2 inside and outside the groove while proportional straining is maintained outside the groove, M-K have shown that deformation within the groove occurs at a faster rate than the rest of the sheet. The concentration of strain (ε_1) within the groove eventually leads to the plane strain condition ($d\varepsilon_2 = 0$) within the groove and to localized necking. The M-K model is thus able to explain localized necking under biaxial as well as uniaxial stresses.

An attractive feature of the M-K analysis is that the concept of the imperfection allows one to interpret both the negative and positive sides of a forming limit diagram ($-\frac{1}{1+R} \leq \varepsilon_2/\varepsilon_1 \leq 1$) in terms of a single criteria (as opposed to relying on Hill's theory for $-\frac{1}{1+R} \leq \varepsilon_2/\varepsilon_1 \leq 0$ and another criteria for biaxial tension). In the M-K analysis, localized necking is developed from the strain concentration within a material imperfection in the form of a groove which is assumed to align <u>perpendicular</u> to the major principal strain axial (ε_1). In biaxial straining of sheet metal $\varepsilon_1 > \varepsilon_2 > 0$), localized necking does occur normal to the major principal strain axis, as assumed in the M-K analysis. However, localized necking usually occurs at an angle <u>inclined</u> to the major principal strain axis when the loading places the strain path in the negative minor strain regime of the forming limit diagram (i.e., $\varepsilon_2/\varepsilon_1 < 0$). The angle of inclination depends on the state of stress as well as plastic anisotropy and thus the R-value of the material. For a plastically isotropic material in uniaxial tension, localized necking occurs inclined to the stress axis at an angle of about 55°, which differs considerably from the 90° assumed by M-K.

This paper suggests an alternative and efficient method of predicting the limit strain of sheet metal failed by localized necking inclined to the σ_1 axis. In this analysis, which is closely related to calculations of

Hutchinson and Neale (13), the orientation of the inclined groove is rigidly fixed along Hill's angle of zero-extension (8). The calculations assume a Swift type constitutive stress (σ) - strain (ε) relationship $\sigma = K(\bar{\varepsilon}_o + \bar{\varepsilon})^n \dot{\bar{\varepsilon}}^m$ and a sheet specimen with an imperfection of size $f = K_B t_B / k_A t_A$, where the subscripts A and B refer to the strength parameter k and thickness t outside or within the imperfection, respectively. The effective strain within the imperfection $\bar{\varepsilon}_B$ may then be related to that outside the imperfection $\bar{\varepsilon}_A$ by:

$$d\bar{\varepsilon}_A^{\,m} [\bar{\varepsilon}_o + \bar{\varepsilon}_A]^n \exp[-C\bar{\varepsilon}_A] = f[\bar{\varepsilon}_o + \bar{\varepsilon}_B]^n \exp[-F \cdot \bar{\varepsilon}_B] d\bar{\varepsilon}_B^{\,m}$$

where

$$F = \sqrt{\frac{3}{2}} \sqrt{\frac{1+2R}{(R+2)(R+1)}} [1+2(R+1)\ \alpha_2^2]^{-\frac{1}{2}}$$

$$C = \sqrt{\frac{3}{2}} \sqrt{\frac{1+2R}{(R+2)(R+1)}} [1+2(R+1)\ \rho_2^2]^{-\frac{1}{2}}$$

and

$$\alpha_2 = \frac{(1-\alpha)\ \sin\phi^* \cos\phi^*}{\cos^2\phi^* + \alpha \sin^2\phi^*} \quad ; \quad \alpha = \frac{\sigma_2}{\sigma_1}$$

$$\rho_2 = \frac{(1-\rho)\ \sin\phi^* \cos\phi^*}{\cos^2\phi^* + \rho \sin^2\phi^*} \quad ; \quad \rho = \frac{\varepsilon_2}{\varepsilon_1}$$

Calculations of forming limits predicted by the inclined groove model indicate that, for a given strain state, the limit strain increases with increasing work hardening rate n, the strain rate hardening exponent m, the plastic anisotropy parameter R, but decreased with increasing imperfection size (i.e., as f becomes smaller); this is demonstrated in Fig. 4. The inclined imperfection model has been found to be much less sensitive to the imperfection factor f, than that of the M-K analysis with a perpendicular imperfection. When applied to the calculation of the uniaxial and forming limit strains of various steels, aluminum alloys, 70-30 brass and CP Ti in the negative minor strain regime, the inclined imperfection model gives better agreement with the experimental results than Hill's theory (8) or the original M-K analysis (9). Especially for the case of uniaxial tension, Hill's

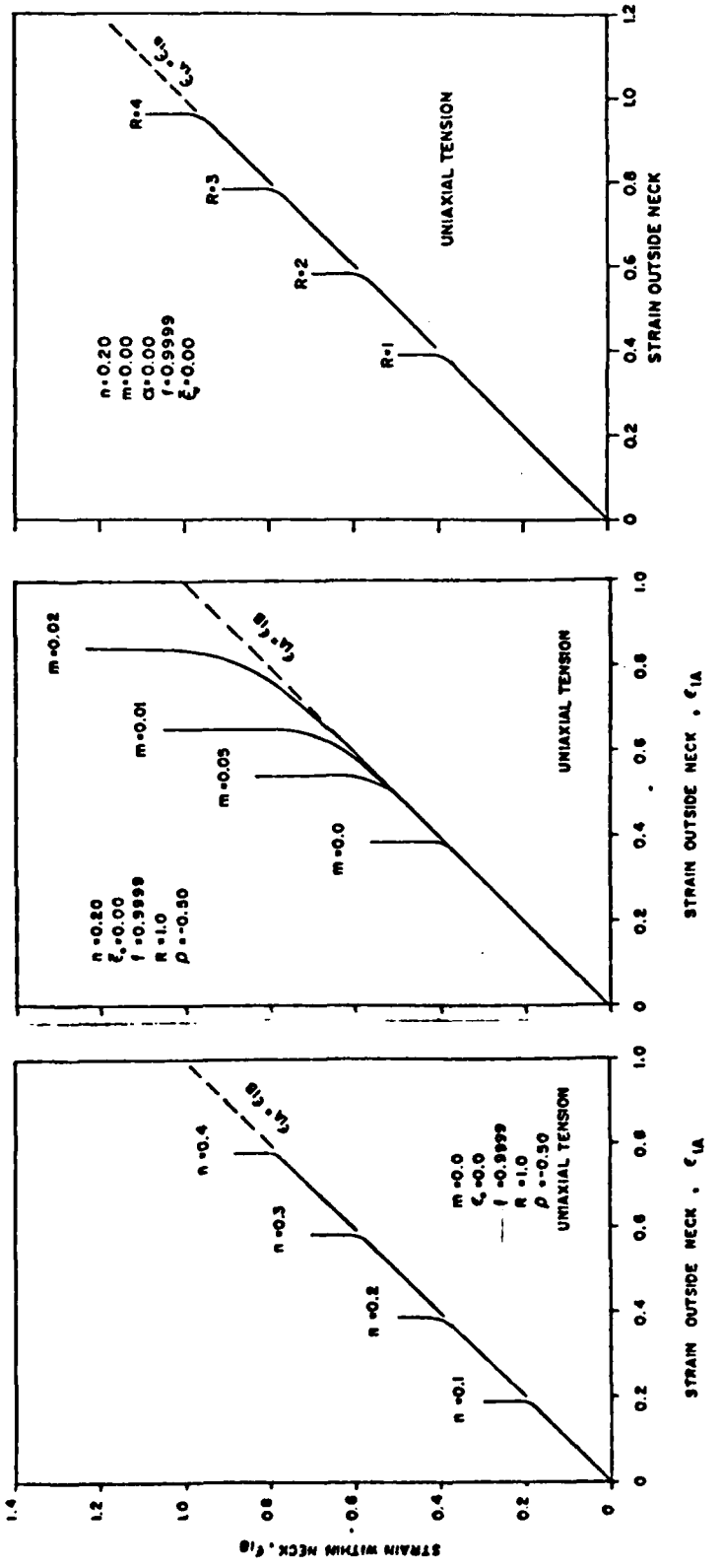

Fig. 4. Strain localization for sheet metal deformed in uniaxial tension as influenced by: (a) the work hardening exponent n, (b) the strain rate sensitivity exponent m, and (c) the plastic anisotropy parameter R. The calculations are based on the inclined imperfection model.

theory tends to overestimate the limit strain when m = 0 but underestimate it when m > 0. Because it involves a change in stress ratio within the imperfection which strengthens it during straining even for $\rho < 0$, the M-K analysis, on the other hand, predicts a limit strain which is either too large or requires an imperfection factor that is unrealistically large.

3) A "Fracture Limit Diagram" for Determining Hydrogen Embrittlement of Sheet Under Multiaxial Loading Conditios
(with R. J. Bourcier, currently Ph.D. candidate, Michigan Tech. Univ.)

Hydrogen embrittlement (HE) has been studied extensively under conditions in which many environmental and metallurgical parameters have been controlled. However, nearly all the studies to date rely on imposing tensile states of stress which are either uniaxial (typically tension or bending) or, on a local scale, strongly triaxial as a result of the presence of a notch or crack. Studies of HE under multiaxial stress states other than notched or pre-cracked plates have been primarily confined to disc pressure tests in which the pressure required to burst clamped metal discs is measured (14-18). However, implicity in all theories of fracture is a fracture criterion which is typically based on a critical stress, strain, or strain energy density. Although burst tests have been very useful in indicating sensitivity of HE to biaxial loading, such studies report burst pressures and not a critical stress (or strain) for fracture. Thus, our present understanding of the influence of stress or strain state on HE is limited because it must rely primarily on a comparison of two relatively extreme cases: simple tension vs. pre-cracked or notched plates.

The purpose of this research is to present an alternative method of determining the HE of sheet material subjected to multiaxial deformaiton (19). Based on the application of punch-stretch testing to HE, the method involves the stretching of gridded sheet over a usually hemispherical punch. The test

procedure allows one to measure, sequentially or at fracture, the principal strain components in the plane of the sheet for any multiaxial deformation losses of ductility, the resulting data may be expressed in the form of a "fracture limit diagram" which identifies a strain criterion for fracture over the complete range of loading paths from uniaxial tension to balanced biaxial tension.

The test method recognizes that stretching is a very common mode of multiaxial deformation in sheet metal forming. As a means of assessing the stretchability of a metal, Hecker has developed a punch-stretch test in which a clamped sheet is stretched to failure over a hardened steel punch (5-7). Fig. 5 schematically shows such a test.

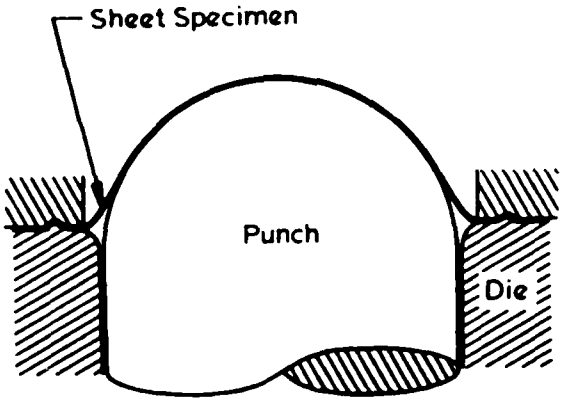

Fig. 5. A schematic diagram of the punch-stretch apparatus.

The punch itself is usually hemispherical but may be flat. The sheet is clamped securely between the die plates, usually with a V-shaped groove and matching draw beads machined into plates to prevent drawing of the specimen. Care must be taken in HE studies so that the plane strain deformation caused by the sheet bending over the draw bead does not cause premature fracture of the specimen.

In order to determine the state of strain in the sheet either during deformation or after fracture, the specimens themselves are gridded with

contacting circles or squares, which may be etched or photographically printed using a photo-sensitive resist method. Grids of this type can be applied with precision on a scale of ~0.5mm and do not affect the deformation or fracture behavior of the specimen. For HE studies, care must be taken to protect the grids during testing in any environment which might degrade them or the metal substrate. The use of grids in the form of circles is especially well suited for strain measurements; from a deformed circle (ellipse), the major (ε_1) and minor (ε_2) principal strains in the plane of the sheet are readily determined. In the case of fracture, the magnitude of ε_1 across the fractured surface can be determined either "directly" from fractured grids or "indirectly" by measuring the width strain ε_2 (from the deformed grids), the thickness strain ε_3, and assuming constant volume in which case: $\varepsilon_1 = -(\varepsilon_2 + \varepsilon_3)$. Measuring ε_1 directly from the fractured grids always introduces an error caused by any strain gradient which may exist over the scale of the grids. However, in many cases such measurements can be made with greater accuracy and are more reproducible than those based on the thickness strain which must rely on often irregular fracture surface profiles. Given a sufficiently small grid (< 1mm), experiments indicate that the two methods of obtaining ε_1 provide data showing identical trends.

Fracture of sheet specimen over the entire range of strain ratios which permit thinning can readily be achieved by controlling the degree of lubrication between the punch and the specimen or by testing strip specimens of reduced width. For example, testing a full width specimen which is well lubricated with several teflon sheets or polyurethane rubber results in loading paths near that of balanced biaxial tension ($\varepsilon_1 = \varepsilon_2$), such as in a hydraulic bulge test. On the other hand, testing specimens of reduced width (i.e., the specimen width is less than the punch diameter) results in a strain

path between pure tension and plane strain. A series of tests of sheet specimens of various widths and under a range of lubrication conditions will determine all possible combinations of fracture strain components which are associated with thinning of the sheet.

The fracture limit diagram is simply a type of fracture map, which in terms of ε_1 and ε_2, identifies the strain components in the plane of the sheet at failure. All strain paths which cause sheet thinning are reported. This ranges from simple tension (in which case $\varepsilon_1 = -\frac{1}{2}\varepsilon_2$ for a plastically isotropic material), through plane strain ($\varepsilon_2 = 0$), and to balanced biaxial tension ($\varepsilon_1 = \varepsilon_2$). A fracture limit diagram for HE will thus normally consist of two or more data curves, one of which represents "hydrogen-free" behavior while the other(s) report failure strain in terms of ε_1 and ε_2 for the embrittled material.

In applying punch-stretch testing to HE studies, the reader should recognize certain advantages as well as disadvantages. The tests are particularly well suited for those HE phenomena which are manifested by a loss of ductility. The loss of ductility may be a result of a decrease in the strain for the onset of localized necking (in which case local necking strains, not fracture strains, should be reported) or, more likely in the case of HE, it will reflect the intervention of a fracture prior to localized necking. In either case the state of strain at failure as well as strain distribution can be readily measured over a range of strain paths ranging from uniaxial to balanced biaxial. The test itself is not easily performed in air; as such, it is most conducive for examining specimens containing internal hydrogen. However, the die and the specimen may be used as a container for either a gaseous or aqueous hydrogen-producing environment so that an external hydrogen study may also be performed. Research of this nature is currently in progress in our department. It should be noted that, although the strain components are experimentally determined,

the stress components cannot be measured because of an unknow degree of friction between the punch and the sheet. One can, however, calculate approximate values of the stresses using plasticity theory and knowing the strain components.

4) Hydrogen Embrittlement of Ti Sheet Under Multiaxial Deformation

(with Roy J. Bourcier, currently Ph.D. candidate, Michgan Tech. Univ.)

Given the unique nature of applying punch stretching to HE studies, we describe here an example of a fracture limit diagram which illustrates a case in which HE is sensitive to loading path. Commercially pure (CP) Ti sheet (~0.8mm thick, 15μm grain size, and 1460 wt ppm oxygen) has been tested in an annealed condition (60 wt ppm H) and after thermal charging to 980 wt ppm H, in which case a considerable amount of titanium hydride is present. Fig. 6 is a fracture limit diagram which reports the limiting fracture strains as measured directly from a 1mm square gridded element of material which includes the fracture surface. Similar data curves, but with each displaced to higher strain levels by a factor of 1.2 - 1.2, are obtained if thickness strains are used to calculate indirectly a true factor strain across the fracture surface.

Previous studies have shown CP Ti to be relatively immune to HE under slow strain rate, simple tension test conditions (10,12). This is confirmed in the fracture limit diagram shown in Fig. 6 for the conditions of ε_1 and ε_2 corresponding to unaxial tension. In contrast, Fig. 6 also indicates that a substantial loss of ductility occurs if hydrogen-charged Ti sheet is deformed under balanced biaxial tension. Under biaxial tension, loss of ductility, in terms of the equivalent strain to fracture $\bar{\varepsilon}_f^*$, becomes substantial: $\bar{\varepsilon}_f^*$ = 51%

*The equivalent strain at fracture $\bar{\varepsilon}_f$ is calculated using Hill's original theory (23) given that the ratio of width strain to thickness strain in a tension test is 2.2 in the transverse direction for both materials, whil in the rolling direction is 5.5 for the sheeting containing ppmH and 4.6 at 9[illegible] ppmH. The magnitude of $\bar{\varepsilon}_f$ in Fig.3 is based on a 1mm element of material which includes the fracture surface and is measured via fracture grids.

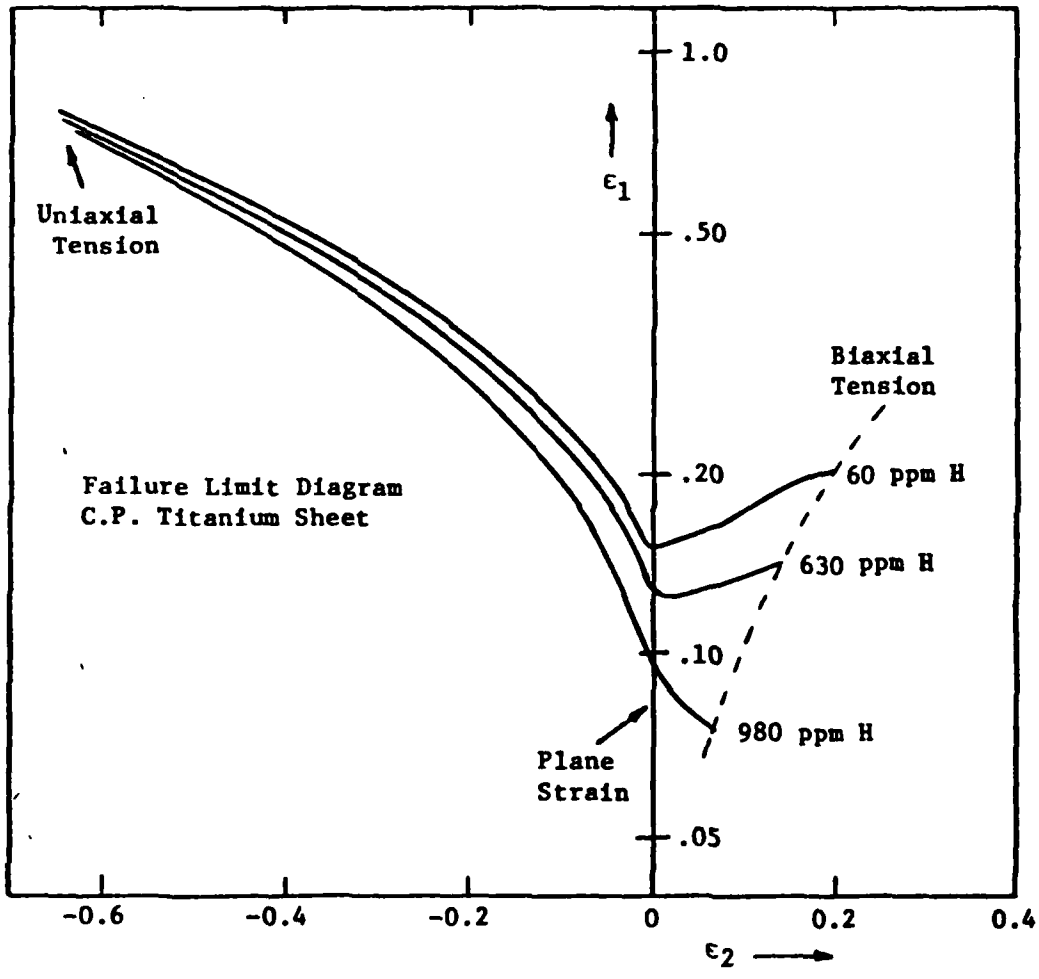

Fig. 6. A failure limit diagram illustrating the influence of loading path on the principal strains at fracture (ε_1 and ε_2) for as-received C.P. Ti sheet containing: 60, 630, and 980 ppm H.

for the Ti containing 60 ppm H but only 20% at 980 ppm H. This behavior is quite consistent with the increased notch sensitivity of CP Ti bar stock charged with hydrogen (20,21); however, it is difficult to separate strain rate effects from stress state effects in such tests.

Fig. 6 also shows a significant loss of ductility occurs in the hydrogen-charged CP Ti sheet under plane strain conditions (ε_2=0): $\bar{\varepsilon}_f$ = 25% at 60 ppm H but only 13% at 980 ppm H. Thus sheet metal forming operations which typically involved near-plane strain deformation, such as bending, will be deleteriously affected by this HE effect. In fact, problems of this sort have arisen and have been diagnosed in terms of the loss of ductility of CP Ti due to HE under multiaxial loading conditions (24). Although the stress state is much different, crack-tip plasticity also depends on plane strain deformation in most cases. Fig. 6 indicates that, even under the reduced plastic constraint of sheet deformation, the loss of ductility in plane strain of the hydrogen-charged CP Ti is sufficient to indicate a loss of fracture toughness due to HE of CP Ti in plate form.

The mechanism responsible for the HE of CP Ti sheet under biaxial tension conditions is presently under investigation. The sensitivity of HE to stress state appears to be related to hydride fracture. Optical and electron microscopy shows that it is the fracture of the hydrides which initiates voids; these subsequently link-up to cause ductile fracture. For reasons not clear at this time, the plastic strain at which hydrides fracture is quite sensitive to loading path. Table I shows that the equivalent shear strain $\bar{\varepsilon}_f$ which results in hydride fracture is only about 15% in plane strain but about 33% in uniaxial tension. Thus the HE of CP Ti due to plane strain and biaxial loading is due to the fracture of the hydrides at smaller strains under these stress states.

Table I. A comparison of the equivalent shear strain at which hydride fracture occurs in a CP Ti alloy containing 980 ppm H. Strains are measured from a 0.5mm square element of material which includes the fracture surface.

Material	Uniaxial	Strain Path Plane Strain	Biaxial
CP Ti + 980 ppm H	$\bar{\varepsilon}_f$ = 33%	15%	22%

5) The Effect of Hydrogen on the Multiaxial Stress Strain Behavior of Titanium Tubing
(with Charles Lentz, M.S. candidate, Michigan Tech. Univ.)

The previous study identifies the sensitivity of hydrogen embrittlement of Ti sheet to the stress state (19). In an effort to determine whether this effect is related to a change in deformation behavior as a function of loading path, the effect of internal hydrogen on the multiaxial stress-strain behavior of commercially pure titanium has been studied.

Thin-wall (.5mm) tubing specimens containing ∿20 or ∿1000 ppm hydrogen have been tested in five different stress path involving tension and/or internal pressure. Both the 20 and 1000 ppm H material exhibit yield surfaces which are in good agreement with those predicted by the Hill criterion for an anisotropic material. The Ti-1000 H material, which contains hydrides, yields at a ∿10% lower effective stress for all given loading paths examined. This effect is believed to be due to the presence of deformation zones introduced by the nucleation and growth of hydride precipitates. As shown in Fig. 7, for strains $\gtrsim$ .02 the flow stress is only slightly affected, if at all, by the hydrides. We thus conclude that the previously observed hydrogen embrittlement of Ti under multiaxial loading is not due to any large change in stress-strain behavior in biaxial or plane strain tension. Biaxial hardening* was observed

*The term "Biaxial hardening" refers to the effective flow stress at a given effective strain in balanced biaxial tension being displaced to higher values when compared to uniaxial or hoop tension.

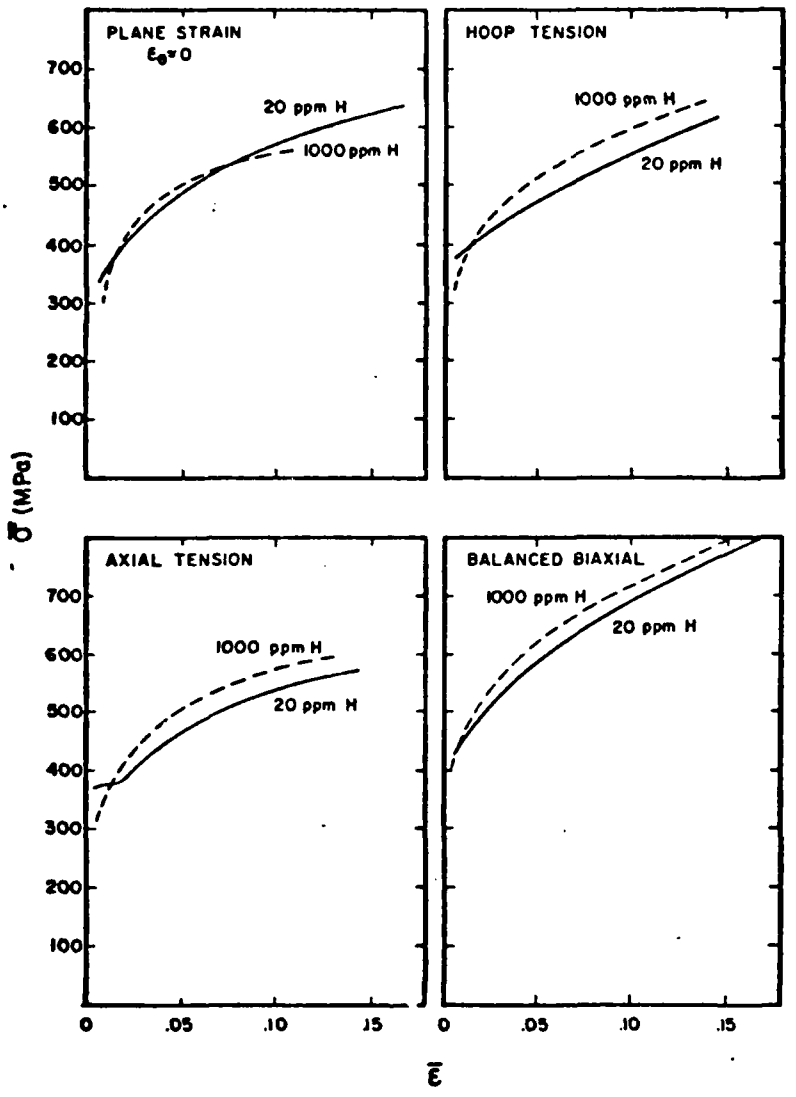

Fig. 7. The Von Mises effective stress-strain curves comparing titanium specimens containing 20 ppm H and 1000 ppm H tested in four differing tension-tension stress states.

in specimens containing both 20 and 1000 ppm H. This hardening effect can be readily understood in terms of the difficulty of through-thickness slip due to the mild crystallographic texture present in the tubes. Twinning was not observed to any large extent and was always less than 3% by volume of the deformed microstructures.

6) The Influence of Hydrogen on the Multiaxial Deformation of a Bcc Titanium Alloy
(with Barbara Lograsso, M.S. Candidate, Michigan Tech. University)

Previous results (see Table I) indicate that the HE of CP Ti sheet under multiaxial loading conditions is caused by the fracture of hydrides at smaller strains in plane strain or balanced biaxial tension when compared to simple tension. In contrast, beta (bcc) Ti alloys have a very high solubility limit for atomic hydrogen. Thus HE effects in beta Ti alloys must usually be interpreted in terms of the presence of hydrogen as a solid solution species (as is also the case in most fcc or bcc alloys). We are thus examining the influence of multiaxial loading path on the HE behavior of β-phase Ti-30V alloys. Sheet specimens of this alloy containing either 35 or 2000 ppm H (which is still well below the solubility limit) are being tested in a range of deformation paths from simple tension to balanced biaxial tension using the techniques described earlier (19). In uniaxial tension, hydrogen causes a small decrease in work hardening but a small increase in the strain rate hardening. The net effect is a small decrease (14% vs. 11%) of the elongation to failure but a small increase in the true strain to fracture measured at the fractured surface ($\sim$1.17 vs. 1.35) as hydrogen content is increased. Preliminary fracture limit diagrams indicate that, unlike the HE of α-phase Ti shown in Fig. 6, there is no pronounced effect of stress state on the HE of the beta Ti alloy. Failure of the sheet is controlled by localized necking, the onset of which appears unaffected by hydrogen.

Acknowledgements

This program is supported by the Office of Naval Research through Contract No. N00014-76-C-0037, NR 031-756.

References

1. K. Okazaki, M. Kagawa, and H. Conrad, Acta. Met. 27, 301 (1979).

2. K. Okazaki, M. Kagawa, and H. Conrad, in Titanium '80 (TMS-AIME, Warrendale, PA), 1980, p. 863.

3. S. S. Hecker in Experimental Studies of Sheet Stretchability (TMS-AIME, Warrendale, PA), 1978, p. 150.

4. K. S. Chan, A. K. Ghosh, and D. A. Koss, "Localized Necking, An Inclined Imperfection Model", Tech. Rep. No. 15, Office of Naval Research Contract N00014-C-76-0037, July, 1981.

5. S. S. Hecker, Met. Eng. Quart. 14, 30 (1974).

6. S. S. Hecker, Sheet Metal Industries, 671 (1975).

7. A. K. Ghosh and S. S. Hecker, Met. Trans. 6A, 1065 (1975).

8. R. Hill, J. Mech. Phys. Solids, 1, 19 (1952).

9. Z. Marciniak and K. Kuczynski, Int. J. Mech. Sci., 9, 609 (1967).

10. S. Stören and J. R. Rick, J. Mech. Phys. Solids, 23, 421 (1975).

11. A. Needleman and N. Triantatyllidus, Trans. ASME, 100, 164 (1978).

12. R. Sowerby and J. L. Duncan, Int. J. Mech. Sci., 13, 217 (1971).

13. J. W. Hutchinson and K. W. Neale, in Mechanics of Sheet Metal Forming (edited by D. P. Koistinen and N. M. Wang), 127; 269, Plenum Press (1978).

14. J.P. Fidelle, R. Broudeur, C. Pirrovani, and C. Roux in Hydrogen Embrittlement Testing, ASTM STP 543, (ASTM, Philadelphia), 1974, p. 34 and 221.

15. J. P. Fidelle, R. Broudeur, and C. Roux, in Effect of Hydrogen on Behavior of Materials, (The Met. Soc. of AIME, New York), 1976, p. 91 and 507.

16. Symposium on The Disc Pressure Tests, Instruments SA-CEA, 91680 Bruyeres-le-Chatel, France (1976).

17. R. P. McNitt, R. D. Sisson, M. R. Louthan, B. A. Lewis, J. MUrali, and J. A. Wagner, in Hydrogen Effects in Metals, p. 785, (The Met. Soc. of AIME, New York), 1981, p. 785.

18. M. R. Louthan, R. D. Sisson, R. P. McNitt, and P. E. Smith in Hydrogen Effects in Metals, (The Met. Soc. of AIME, New York), 1981, p. 829.

19. R. J. Bourcier and D. A. Koss, "A'Fracture Limit Diagram' for Determining Hydrogen Embrittlement of Sheet Under Multiaxial Loading Conditions," ONR Tech. Rep. No. 16, Contract No. N00014-76-C-0037, Sept., 1981.

20. G. A. Lenning, C. M. Craighead, and R. I. Jaffee, Trans. AIME 200, 367 (1954).

21. R. I. Jaffee, G. A. Lenning, and C. M. Craighead, Trans. AIME 206, 907 (1954).

22. C. J. Beevers and D. V. Edmonds, Trans. AIME, 245, 2391 (1969).

23. R. Hill, The Mathematical Theory of Plasticity, p. 318, Oxford Press, Oxford, 1950.

24. J. A. Hall, unpublished research, 1980.